Tuning of $L1_0$ atomic order in Co-Pt nanoparticles: *Ab initio* insights

Roman V. Chepulskii* and W. H. Butler

Center for Materials for Information Technology, University of Alabama, Tuscaloosa, Alabama 35487, USA

(Received 27 September 2011; revised manuscript received 19 December 2011; published 1 October 2012)

Monte Carlo simulation of the atomic configurational behavior of Co-Pt nanoparticles is performed in wide temperature-composition-size ranges. The simulation is based on bulk and local (inhomogeneous) cluster expansions calculated from first principles. A sharp drop of equilibrium $L1_0$ order is predicted for small equiatomic particles at low temperatures. This drop is explained by the interplay of two effects. First, the strong Pt and Co segregation to the first and second surface layers, respectively (core/Co/Pt or "onion2shell" profile) cause a depletion of Pt atoms within the core of small Co-Pt particles. Second, $L1_0$ is an adaptive structure on the fcc-restricted ground-state phase diagram of Co-Pt. Nevertheless, we show that a remarkable degree of $L1_0$ order can be restored by tuning the total composition of small Co-Pt particles.

DOI: 10.1103/PhysRevB.86.155401 PACS number(s): 75.50.Tt, 61.46.Hk, 64.70.Nd, 61.66.Dk

I. INTRODUCTION

Bulk equiatomic Fe-Pt and Co-Pt alloys transform into the $L1_0$ atomic structure at relatively low temperatures.[1] The high spatial anisotropy of the $L1_0$ structure combined with strong spin-orbit coupling on the high-Z Pt site produces a high magnetic anisotropy.[2–5] This high anisotropy makes Fe-Pt and Co-Pt possible candidates for next-generation recording media and high-performance permanent magnets based on monodisperse nanoparticles.[6–17]

Although experimental studies have exposed difficulties in achieving $L1_0$ order in small nanoparticles,[8,9,13] theoretical studies[18–26] have predicted that the $L1_0$ structure should be observed even in small equilibrium nanoparticles. It was theoretically concluded[18–20] that the experimental difficulties in achieving $L1_0$ order should be attributed to kinetic issues. In later experiments, the kinetic obstacles were successfully overcome by use of NaCl, amorphous carbon and aluminum, ion irradiation, larger annealing temperature, and time.[14–16,26–35]

Theoretical studies of atomic order-disorder transformations in Co-Pt nanoparticles were reported in Refs. 25 and 26, in which the many-body tight-binding potential was empirically fitted to experimental data on bulk alloy formation enthalpies and then applied in Monte Carlo simulations. The obtained results on $L1_0$ order in Co-Pt were found to be qualitatively similar to those in Fe-Pt.[18–24] However, Co surface segregation was predicted, which is in contrast to experimental[36] and theoretical data.[37–45] In addition, the bulk order-disorder transition was predicted[46] to be 762 K, which is substantially lower than the corresponding experimental value of 1100 K.[1,47–49] In Refs. 50 and 51, the size-dependent transition temperatures in Co-Pt were estimated semiphenomenologically using a mean-field approximation and finite-size scaling.[50] The estimation used the data on completely ordered $L1_0$ and disordered $A1$ structures obtained from the Korringa-Kohn-Rostoker coherent-potential approximation[50] (KKR-CPA) and the generalized-bond-energy model.[51]

In this paper, we employ the formalism developed by Chepulskii *et al.* in Refs. 18–20. The bulk[52–55] and local (inhomogeneous)[20,56–58] cluster expansions are obtained from first principles. The cluster expansions are used for explanation of atomic interactions both in the core and at the surface of the nanoparticle. Using the cluster expansions within Monte Carlo simulations, the $L1_0$ order in Co-Pt truncated octahedrons is studied for wide temperature-composition-size ranges.

II. COMPUTATION DETAILS

The quantum mechanical energies are calculated from first principles within the generalized gradient approximation[59] using projector augmented wave pseudopotentials, as implemented in the VASP package.[60] Calculations are performed at zero temperature, and without zero-point motion. The effect of lattice vibrations is omitted. Perfect fcc-based configurations are used as the starting point for further relaxations. Numerical convergence to within about 1 meV/atom is ensured by enforcing a high-energy cutoff (400 eV) and dense Monkhorst-Pack **k**-point meshes equivalent to a $16\times16\times16$ mesh for a fcc cubic unit cell. The smearing width of 0.2 eV was applied at Fermi level within the method of Methfessel-Paxton.[61] Only the Γ point is used in the direction perpendicular to the slab. All structures are considered as potentially ferromagnetic and are fully relaxed (cell shape and volume, collinear spins, and atom cell-internal positions). The empty space between the slabs is maintained at $\sim$12 Å.

The configurational behavior of Co-Pt nanoparticles is described by a combination of bulk[52–55] and local (inhomogeneous)[20,57,58] cluster expansions within the approach suggested in Refs. 18–20. The cluster expansions are based on the lattice gas model.[62–66] A finite-temperature Monte Carlo simulation scheme is used as in Refs. 18–20. Periodic and free boundary conditions are applied for the case of bulk and truncated octahedron simulations, respectively. The number of Monte Carlo steps toward the equilibrium state and for averaging are varied depending on the system size and temperature. While spanning the phase space, $L1_0$ order is monitored by the order parameter $\overline{\eta}$ defined in Ref. 20:

$$\overline{\eta} = \langle \max\{|\eta_x|,|\eta_y|,|\eta_z|\} - \min\{|\eta_x|,|\eta_y|,|\eta_z|\} \rangle, \quad (1)$$

where $\langle \ldots \rangle$ is the statistical average over the Monte Carlo steps, and the three directional parameters η_i $(i = x,y,z)$ are defined as the difference between the Pt atom concentrations at odd and even crystal planes perpendicular to the ith direction.

III. BULK EQUIATOMIC CLUSTER EXPANSION

The Pt unary $V^{(1)}$ and pair $V_s^{(2)}$ lattice potentials of the bulk equiatomic cluster expansion are determined from a set of N_ε linear equations:[19]

$$\varepsilon_i = V^{(1)} c_i + \sum_{s=1}^{N_s} S_{is} V_s^{(2)}, \quad i = 1,2,\ldots,N_\varepsilon, \tag{2}$$

where

$$\varepsilon_i = E_i^{\text{at}} - E_{\text{Co,fcc}}^{\text{at}}, \tag{3}$$

E_i^{at} and $E_{\text{Co,fcc}}^{\text{at}}$ are the energies (per atom) of ith structure and pure fcc Co calculated from first principles (see Sec. II), S_{ij} are the structural coefficients, c_i is the concentration of Pt atoms in ith structure, N_ε and N_s are the total numbers of input structures and pair interactions within the cluster expansion. All N_ε input structures have equiatomic composition $c_i = 0.5$. Thus, the approach corresponds to the canonical cluster expansion formalism.[67–69] Pure Co is considered in the fcc state because the considered cluster expansion is fcc based. Note that the choice of Co or Pt as a reference state in our cluster expansion is arbitrary and gives equivalent results.

In Tables I and II, we present the results of bulk *ab initio* calculations for all considered structures. Table II demonstrates that the lattice parameter and tetragonality ratio obtained for the $L1_0$ structure are in good agreement with the corresponding values calculated and measured elsewhere. However, the formation enthalpy, while in good agreement with other theoretical data, differs significantly from the experimental value.

We use the same $N_\varepsilon = 23$ equiatomic input structures as in Refs. 18 and 19 for calculation of bulk cluster expansion (i = 1–23 in Table I). In Fig. 1, we evaluate the cross validation (CV), least-squares fitting (LSF) errors,[19,55] and order-disorder transition temperatures for eight bulk cluster expansions with $N_s = 1,2,\ldots,8$ pair interactions. The corresponding pair potentials $V_s^{(2)}$ and their Fourier transforms $V_{\mathbf{k}}^{(2)}$ are presented in Fig. 2. The minimum CV error (5.6 meV) is obtained for $N_s = 4$. Good convergence of the LSF error (4.6 meV) of the order-disorder transition temperature (485–490 K), and of the pair potential is also achieved at $N_s = 4$.

In Fig. 3, we compare the structural energies predicted by the bulk cluster expansion ($N_s = 4$) to those obtained directly from first principles. In addition to the 23 input structures used for calculation of the cluster expansion, we also evaluated additional 13 equiatomic and 4 nonequiatomic structures (see Table I). The obtained *equiatomic* bulk cluster expansion demonstrates good predicability for *equiatomic* structures. Moreover, we also obtained satisfactory numerical accuracy for 4 near-equiatomic structures. This allows us to use the obtained equiatomic cluster expansion in the vicinity of equiatomic composition as well (see Sec. V).

Based on the obtained results, we consider the bulk cluster expansion at $N_s = 4$ as the most appropriate for configurational description of bulk equiatomic and near-equiatomic Co-Pt. The numerical values of this cluster expansion are listed in Table III. Note that the use of $N_\varepsilon = 36$ (taking all equiatomic structures as input) instead of $N_\varepsilon = 23$ makes negligible changes to the cluster expansion.

TABLE I. The values of ε_i [see Eq. (3)] as well as of the formation enthalpies $\Delta H_{\text{fcc/fcc}}^{\text{at}} = E_i^{\text{at}} - (1-c_i)E_{\text{Co,fcc}}^{\text{at}} - c_i E_{\text{Pt,fcc}}$ and $\Delta H_{\text{hcp/fcc}}^{\text{at}} = E_i^{\text{at}} - (1-c_i)E_{\text{Co,hcp}}^{\text{at}} - c_i E_{\text{Pt,fcc}}$ determined with respect to pure fcc Pt and pure fcc/hcp Co for all considered bulk structures. The first 28 structures are defined in Ref. 19. APB(n) is the $L1_0$ structure with regular parallel antiphase boundaries separated by na distance (a is fcc lattice parameter). The structures 33–35 are A_2B_2 superlattices: V2-(111), W2-(311), Y2-(011). The $D4$ structure is described in Ref. 72. The structures 37–40 are described in the Appendix. All values are in meV.

i	Name	ε_i	$\Delta H_{\text{fcc/fcc}}^{\text{at}}$	$\Delta H_{\text{hcp/fcc}}^{\text{at}}$
		$c_i = 0.5$		
1	$L1_0$	418.8	−98.4	−89.3
2	CH,APB(1)	443.7	−75.6	−66.5
3	APB(2)	424.2	−95.1	−86.0
4		508.3	−11.0	−1.9
5		492.4	−26.8	−17.8
6		503.0	−16.3	−7.2
7		446.7	−68.5	−59.0
8		443.2	−71.9	−62.5
9		440.4	−72.8	−63.6
10		434.4	−78.7	−69.5
11		431.3	−81.8	−72.6
12		450.4	−66.2	−56.5
13		493.7	−21.6	−11.3
14		460.1	−55.2	−44.9
15		464.6	−47.6	−35.7
16		515.7	−3.8	10.2
17		500.0	−19.5	−5.6
18		442.0	−69.7	−64.3
19		454.5	−66.0	−53.0
20		426.0	−92.5	−83.9
21		451.6	−64.9	−55.1
22		452.7	−63.8	−54.0
23		451.6	−67.5	−58.4
24	$Z2$	456.1	−61.0	−52.0
25		444.0	−75.2	−66.2
26		447.8	−71.5	−62.4
27		437.8	−81.4	−72.4
28		436.0	−83.3	−74.2
29	APB(1.5)	432.2	−86.2	−77.2
30	APB(2.5)	423.4	−93.9	−84.9
31	APB(3)	423.0	−96.2	−87.2
32	$L1_1$	473.7	−43.4	−34.4
33	$V2$	498.5	−18.7	−9.7
34	$W2$	437.1	−80.0	−71.0
35	$Y2$	453.8	−63.3	−54.3
36	$D4$	483.0	−34.1	−25.1
		$c_i = 4/9, 5/9$		
37	Co_5Pt_4	365.5	−94.4	−84.4
38	Co_4Pt_5	493.4	−81.4	−73.4
39	Co_5Pt_4	397.9	−61.9	−51.9
40	Co_4Pt_5	489.8	−85.0	−77.0

Our bulk cluster expansion gives 490 K for the Co-Pt order-disorder transition. This is approximately half of the 1100 K measured experimentally.[1,47–49] This result contrasts with the case of Fe-Pt for which 1495 K was predicted within the same formalism and 1572 K was observed experimentally.[19] The CV (5.6 meV) and LSF (4.6 meV) errors for the case of

TABLE II. Lattice parameter a, tetragonality ratio c/a, and formation enthalpy $\Delta H^{\text{at}}_{\text{hcp/fcc}}$ obtained for the $L1_0$ structure in this paper compared with the corresponding values calculated and measured elsewhere.

$L1_0$-FM	a (Å)	c/a	$\Delta H^{\text{at}}_{\text{hcp/fcc}}$ (meV)
Expt.	3.80[a]	0.972[a]	-140.1 ± 22.0[b]
GGA[c]	3.81	0.977	−89.3
Other GGA[d]	3.82	0.973	−88.4
LDA[d]	3.75	0.967	−79.0
KKR-ASA[d]	3.78	0.984	−95.0

[a]Reference 70.
[b]Reference 71.
[c]This study.
[d]Reference 50.

Co-Pt are even less than those of Fe-Pt (13.5 and 10.6 meV, respectively). Thus, the low Co-Pt transition temperature is not a consequence of an insufficiently accurate cluster expansion. The accurate cluster expansion is a mirror of the energies of considered structures. Thus, the low transition temperature is related to those energies. For instance, the formation enthalpy of the $L1_0$ structure (−89.3 meV) and cluster-expansion-based transition temperature (490 K) in Co-Pt are both approximately three times smaller in absolute value than those of Fe-Pt

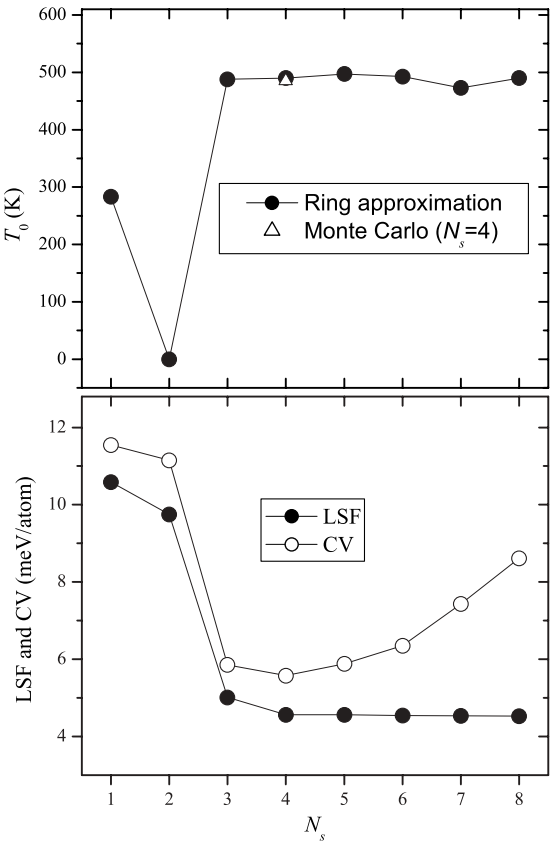

FIG. 1. The values of cross validation (CV), least-squares fitting (LSF) errors (Refs. 19 and 55), and order-disorder transition temperature T_0 vs the number N_s of pair interactions within the cluster expansion. T_0 is obtained within the ring approximation (Refs. 73 and 74) and Monte Carlo simulation (for $N_s = 4$).

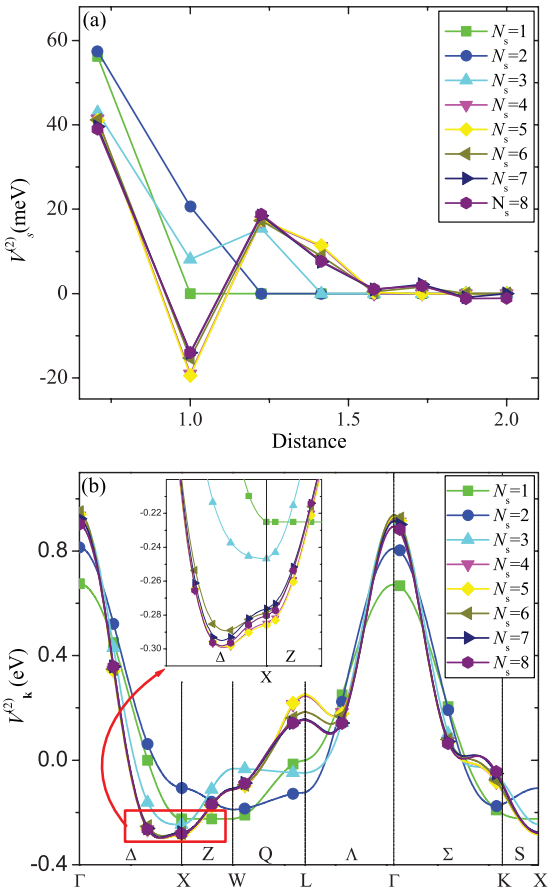

FIG. 2. (Color online) Pair mixing potential $V^{(2)}_s$ in (a) real and (b) reciprocal spaces obtained by cluster expansion fitting to first-principles data at $N_\varepsilon = 23$, $N_s = 1,2,\ldots,8$. The "distance" is measured in fcc lattice parameter units.

(−240.5 meV and 1495 K, respectively). Moreover, as noted above, the calculated and experimentally measured formation

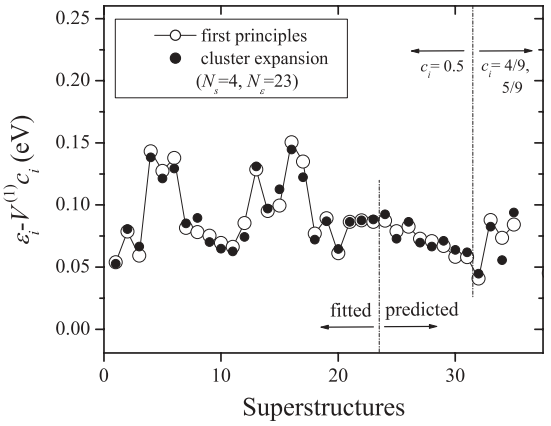

FIG. 3. The values of $\varepsilon_i - V^{(1)}c_i$ [see Eqs. (2) and (3)] for 36 equiatomic ($c_i = 0.5$) and 4 nonequiatomic ($c_i = 4/9,5/9$) structures (see Table I) calculated directly from first principles and through the cluster expansion ($N_s = 4$, $N_\varepsilon = 23$). The difference between two energies characterizes the accuracy of cluster expansion. The first 23 structures are used in the cluster expansion fitting. The other 17 structures (including 4 near equiatomic) assess the predictive power of cluster expansion.

TABLE III. Cluster expansion unary $V^{(1)}$ and pair $V_s^{(2)}$ mixing potentials calculated at $N_s = 4$, $N_\varepsilon = 23$ (see also Fig. 2). The Cartesian coordinates of vector **R** are given in $a/2$ units, where a is the fcc lattice parameter.

s	**R**	$\|\mathbf{R}\|/a$	$V_s^{(2)}$ (meV)
1	110	0.707	41.4
2	200	1.000	−19.0
3	211	1.225	17.4
4	220	1.414	11.2
	$V^{(1)} = 679.7$ meV		

enthalpies of the $L1_0$ structure are substantially different (see Table II).

At higher temperatures, other factors not included in the cluster expansion may become important. For example, the consideration of paramagnetic rather than the ferromagnetic structures considered here may shift the theoretical transition temperature much closer to the experimental one.[50] However, the experimental magnetic phase transition occurs[1,47–49] at considerably higher temperature than the *predicted* atomic order-disorder transition in Co-Pt. Therefore, the "ferromagnetic" cluster expansion should be a reasonable approximation in that temperature region. The vibrational free energy may also contribute at high temperatures,[75] although it usually decreases the transition temperature.[76] The asymmetry of the bulk phase diagram[1,47–49] may be a sign of nonpair interactions.[77] Nevertheless, we consider the obtained cluster expansion to be reliable for qualitative estimation of configurational effects within the most technologically interesting region of low/medium temperatures. In other theoretical simulations of Co-Pt,[25,26,78–82] the predicted bulk order-disorder transition temperatures are substantially lower than those measured experimentally.

From Fig. 2(b), it follows that the absolute minimum of the Fourier transform of the pair potential is located not exactly at the $X = (100)$ **k** point [as in Fe-Pt (Ref. 20)], but rather near it. This feature appears when we take into account four or more shells of atomic interactions ($N_s > 3$). Correspondingly, the X diffuse-intensity peak splits as shown in Fig. 4. This splitting is topologically different from the peak splitting in Cu-Au (Ref. 83) and Cu-Pd.[84,85] Unfortunately, we were not able to find experimental studies of high-temperature monocrystal diffuse scattering at/near equiatomic composition in Co-Pt for a comparison with our theoretical data.

The "non-high-symmetry" global minimum of $V_{\mathbf{k}}^{(2)}$ can be related to long-period structures appearing at low temperatures and/or composition variation.[64,85] Our Monte Carlo simulations indeed reveal secondary phase transitions below the disorder/$L1_0$ transition at nonequiatomic compositions (see Sec. V). This is in accordance with the adaptiveness of $L1_0$ on the fcc-restricted convex hull.[87] The predicted appearance of low-temperature nonequiatomic secondary phases needs further experimental verification.

IV. SURFACE POTENTIAL

The high ratio of surface to core atoms in nanoparticles requires a modification of the bulk cluster expansion by introduction of a surface potential. Following the approach developed in Ref. 20, we consider the Co-Pt nanoparticle as a truncated octahedron, which is the most often observed shape in Pt-based nanoparticles.[10,26,33,35,88–92] The (001), (100), and (111) surfaces of a truncated octahedron with perfect $L1_0$ order are modeled considering three periodic slabs (see Fig. 5). The perfect $L1_0$ slabs are transformed by swapping atoms of different atomic layers. The surface potential is evaluated by comparison of *ab initio* energies of transformed slabs. The corresponding results (marked as "GGA") are presented in Table IV and Fig. 6.

The obtained *ab initio* results already reveal a tendency for Pt surface segregation. This is because the slab energies decrease in all cases when a Pt atom moves to the surface

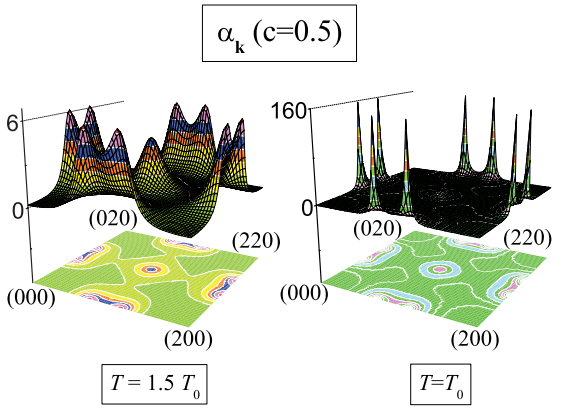

FIG. 4. (Color online) Fourier transforms $\alpha_{\mathbf{k}}$ of the short-range order parameters in $(h,k,0)$ plane of the fcc Brillouin zone. It is calculated within the ring approximation (Refs. 74 and 86) using the bulk cluster expansion from Table III. Equiatomic composition c and two temperatures T are considered. T_0 is the disorder/$L1_0$ transition temperature.

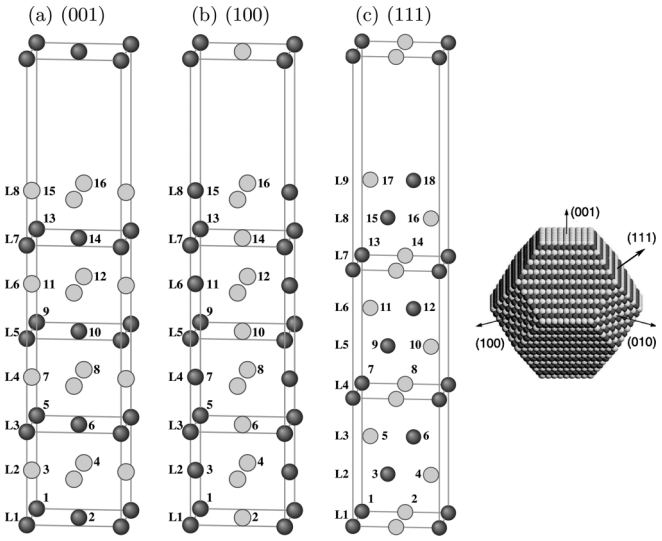

FIG. 5. The unit cells of crystal structures representing atomic slabs separated by vacuum used to model the nanoparticle's facets. Each slab is obtained from an unrelaxed $L1_0$ crystal structure along (a) (001), (b) (100), and (c) (111) planes. Layers (L) and atoms are enumerated. Fe and Pt atoms are marked as black and gray circles, respectively.

TABLE IV. Formation energies of (001), (100), and (111) slabs (relative to perfect $L1_0$) calculated from both first principles (GGA) and using three cluster expansions ("CE"): "aniso2," "so2," and "bulk" (see Table V). The slabs are identified by the label "L_{ij}," where i and j indicate the layers between which the atoms are exchanged (see Fig. 5). Two configurations are considered: ij and $\underline{ij}$ for every choice of i and j. "Atom exchange(s)" describe the difference of slab from the perfect $L1_0$ (see numbering of atoms in Fig. 5).

		$E - E_{L1_0}$			
L_{ij}	Atom exchange(s)	GGA (eV/at)	CE_{aniso2} (eV/at)	CE_{iso2} (eV/at)	CE_{bulk} (eV/at)
		(001), Fig. 1(a)			
78	14↔15	0.035	0.035	0.040	0.012
<u>78</u>	14↔15,13↔16	0.070	0.071	0.081	0.026
67	11↔14	0.021	0.021	0.020	0.006
<u>67</u>	11↔14,12↔13	0.043	0.043	0.041	0.014
56	10↔11	0.008	0.006	0.006	0.006
<u>56</u>	10↔11,9↔12	0.020	0.014	0.014	0.014
45	7↔10	0.008	0.006	0.006	0.006
<u>45</u>	8↔9	0.016	0.014	0.014	0.014
34	5↔8	0.006	0.006	0.006	0.006
<u>34</u>	6↔7	0.011	0.014	0.014	0.014
23	3↔6	0.000	−0.001	−0.001	0.012
<u>23</u>	4↔5	−0.001	0.000	−0.001	0.026
12	2↔3	−0.034	−0.031	−0.034	−0.007
<u>12</u>	1↔4	−0.057	−0.061	−0.066	−0.012
		(100), Fig. 1(b)			
45	7↔10	0.013	0.006	0.006	0.006
<u>45</u>	8↔9	0.013	0.006	0.006	0.006
34	5↔8	0.012	0.006	0.006	0.006
<u>34</u>	6↔7	0.012	0.006	0.006	0.006
23	3↔6	0.018	0.016	0.016	0.002
<u>23</u>	4↔5	−0.004	−0.006	−0.006	0.008
12	2↔3	0.043	0.038	0.040	0.013
<u>12</u>	1↔4	−0.026	−0.031	−0.033	−0.006
		(111), Fig. 1(c)			
45	7↔10	0.019	0.018	0.018	0.018
<u>45</u>	8↔9	0.018	0.018	0.018	0.018
34	5↔8	0.020	0.018	0.018	0.018
<u>34</u>	6↔7	0.019	0.018	0.018	0.018
23	3↔6	0.029	0.029	0.028	0.016
<u>23</u>	4↔5	0.006	0.007	0.008	0.020
12	2↔3	0.056	0.052	0.044	0.020
<u>12</u>	1↔4	−0.019	−0.023	−0.014	0.010

from internal layers of perfect $L1_0$ ("Pt-up" in Fig. 6). When a Pt atom is removed from the surface, the energies increase ("Pt-down" in Fig. 6). The obtained absolute energy gains and losses are larger than in Fe-Pt.[20] So, we expect stronger Pt surface segregation in Co-Pt than in Fe-Pt. This is confirmed below by values of surface potential and by simulations. Pt surface segregation has been observed experimentally[36] and calculated theoretically[37–45] in previous studies. The Co surface segregation obtained in Refs. 25 and 26 can be explained by a sensitivity of segregation tendencies to the choice of atomic potential.[80,81] A stronger Pt surface segregation in Co-Pt than in Fe-Pt may be attributed to a larger difference in atomic radii between Pt and Co than Pt and Fe.

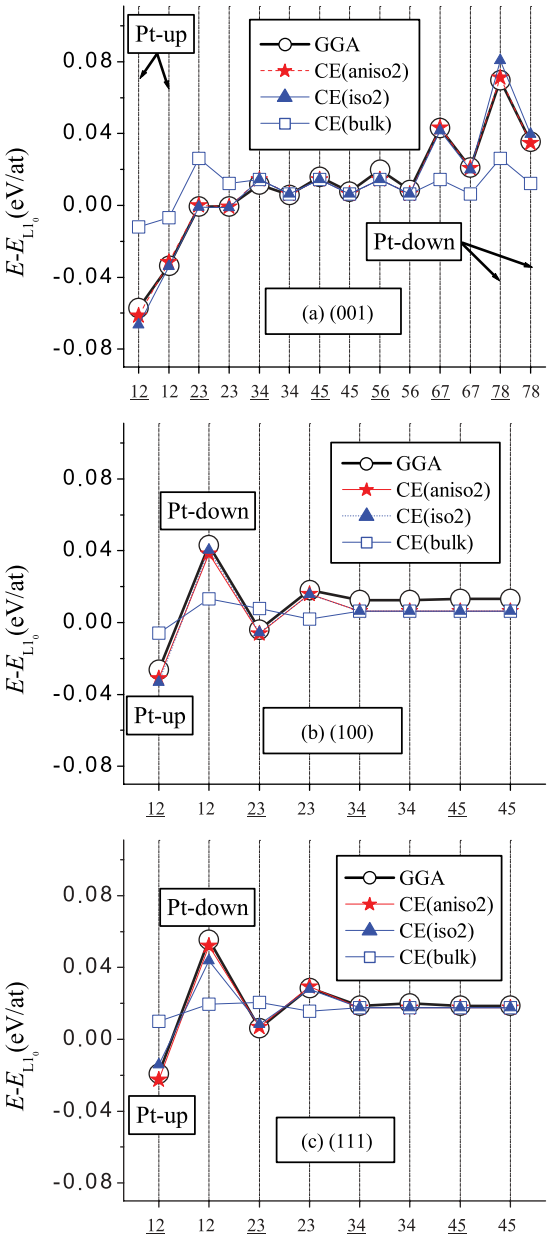

FIG. 6. (Color online) Graphical representation of the data from Table IV. "Pt-up"/" "Pt-down" mean that Pt atoms move to/from the surface of the perfect $L1_0$ slab.

In Table IV and Fig. 6, we also present the same energy differences but given by bulk cluster expansion. Their comparison with *ab initio* data reveals the considerably higher numerical error of the bulk cluster expansion when atomic exchanges in the two outer layers are involved. This illustrates the necessity of cluster expansion modification near the surface. The modification is done by varying the Pt unary lattice potential $V^{(1)}$ as a function of atomic layer to better fit to the slab *ab initio* data. So, formally we add an inhomogeneous external surface potential into the cluster expansion. We consider a number of such local cluster expansions with (a) one or two external atomic layers affected by the surface potential and (b) anisotropic or isotropic surface potentials.

The constructed local cluster expansions are presented in Figs. 6 and 7 and Tables IV and V including the estimation

TABLE V. Cluster expansions obtained for a description of nanoparticle configurational energies. "bulk" is the bulk cluster expansion without accounting for surface effects. "iso1" and "iso2" ("aniso1" and "aniso2") designate the implementation of isotropic (anisotropic) surface potential affecting one and two external layers, respectively. "100iso1" and "100iso2" are the hybrid cluster expansions for which $V^{(1)}_{001} = V^{(1)}_{100} \neq V^{(1)}_{111}$. The least-squares-fitting (LSF) errors characterize the atom exchange energies in two external layers (within each surface and total).

Layers		Cluster expansions						
(*lmn*)	*i*	bulk	iso1	iso2	100iso1	100iso2	aniso1	aniso2
					$V^{(1)} - V^{(1)}_{\text{bulk}}$ (eV)			
(001)	8	0	−0.436	−0.219	−0.386	−0.182	−0.359	−0.157
	7	0	0.000	0.217	0.000	0.204	0	0.202
	2	0	0.000	0.217	0.000	0.204	0	0.186
	1	0	−0.436	−0.219	−0.386	−0.182	−0.395	−0.209
(100)	2	0	0.000	0.217	0.000	0.204	0	0.225
	1	0	−0.436	−0.219	−0.386	−0.182	−0.403	−0.179
(111)	2	0	0.000	0.217	0.000	0.257	0	0.257
	1	0	−0.436	−0.219	−0.587	−0.330	−0.587	−0.330
					LSF error (eV/at)			
(001)		0.026	0.021	0.013	0.020	0.012	0.020	0.004
(100)		0.021	0.011	0.004	0.011	0.004	0.011	0.004
(111)		0.022	0.011	0.008	0.008	0.003	0.008	0.003
Total		0.024	0.017	0.010	0.016	0.009	0.015	0.004

of their accuracy in surface regions. We find that the bulk cluster expansion is affected by the surface potential only at the two external surface layers (see Fig. 7). This agrees with the conclusion of Ref. 40 that migration and formation energies for only two external Co-Pt(100) layers are different from the bulk. The obtained surface potential implies surface segregation of Pt (Co) at the first (second) outer layers. Pt segregation (depletion) in the first (second) surface layers with almost unaffected deeper layers have been observed experimentally.[36]

The bulk cluster expansion LSF error (24 meV) decreases to 15–17 meV when a surface potential for a single outer layer is included. The effect of surface potential anisotropy is small in this case (2 meV). Accounting for the surface potential of the second layer decreases LSF error further to 4–10 meV with a larger anisotropy effect (6 meV).

In the nanoparticle simulations shown in the following, we use the local cluster expansion with a two-layer isotropic surface potential ("iso2"). It gives low LSF error in the surface region (10 meV) comparable with core CV (5.6 meV) and LSF (4.6 meV) errors. The possible use of a two-layer *anisotropic* surface potential ("aniso2") would be considerably more complicated but would not decrease the LSF error very much. In fact, we do not need the surface LSF error to be lower than that of the core. As we show in the following, the obtained surface potential is so strong that Pt and Co atoms occupy almost all lattice sites at the first and second atomic layers, respectively. So, we expect that weak anisotropy would hardly change the observed effects. We believe that such a strong surface potential calculated from near-$L1_0$ structures is unlikely to be much affected by atomic disorder at higher temperatures.

In Co-Pt, the obtained "iso2" surface potential (−0.22 and 0.22 eV at first and second layers, respectively) is stronger than that of Fe-Pt (−0.13 and 0.2 eV).[20] This should imply a stronger rate of surface segregation in Co-Pt than in Fe-Pt. Stronger surface segregation in Co-Pt than in Fe-Pt was calculated directly from first principles.[41,44] In these cases, segregation was stronger for the outer layer in Co-Pt than in Fe-Pt in nanoparticles (with some tendency for Co and Fe to segregate at subsurface layer).

V. MONTE CARLO SIMULATION

A. Bulk

The surface potential makes the atomic composition inhomogeneous within a nanoparticle.[20] In order to better understand the configurational behavior of *non*equiatomic Co-Pt, we first perform bulk Monte Carlo simulation using the bulk cluster expansion. In Fig. 8, the temperature dependencies of the bulk $L1_0$ order parameter at three atomic compositions are presented. It is demonstrated that a considerable decrease in the $L1_0$ order parameter is possible at low temperatures if the composition deviates sufficiently from the equiatomic value. Generally, the $L1_0$ order parameter measured within a non-$L1_0$ structure should be lower than in $L1_0$. In particular, the $L1_0$ order parameter is zero within the $L1_2$ structure. We speculate that this decrease in the $L1_0$ order parameter for $c = 0.40$ corresponds to order-order and/or decomposition phase transitions involving other structures. This is consistent with the "non-high-symmetry" global minimum of $V^{(2)}_{\mathbf{k}}$ (see Sec. III) and with the "adaptiveness" of the $L1_0$ structure related to the low energy of antiphase boundaries.[87]

B. Truncated octahedron

We consider truncated octahedrons of five different sizes described in Table VI. The atomic compositions are chosen to satisfy the condition of perfect $L1_0$ order in the completely ordered state for each particle. Because of the surface geometry, such compositions are close but not equal

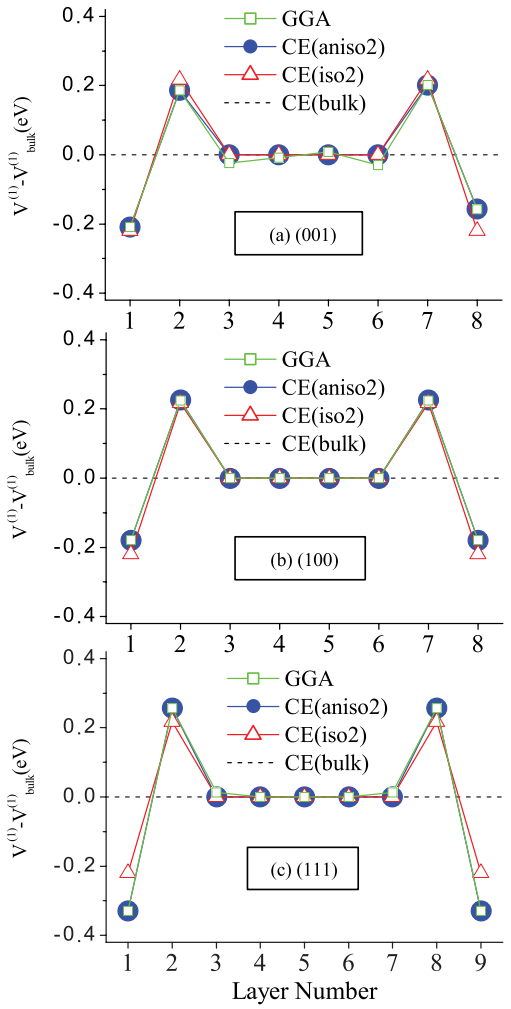

FIG. 7. (Color online) The dependence of relative surface potential on the layer number in (a) (001), (b) (100), and (c) (111) slabs corresponding to initial first-principles (GGA) data and three cluster expansions: "aniso2," "iso2," and "bulk" (see Table V).

to the equiatomic value for the case of small particles. The diameter of a nonspherical particle can be defined in a number of different ways[20,22,50] as presented in Table VI. We determine the diameters by the use of bulk 0.38-nm lattice parameter. Thus, we neglect the lattice contraction due to the surface tension, which may be substantial in case of small particles.[93]

The results of Monte Carlo simulation for truncated octahedrons with near-equiatomic (see Table VI) total compositions are presented in Fig. 9. The "iso2" local cluster expansion is used in all simulations. Figure 9(c) shows very strong Pt and Co segregation at surface (first layer) and subsurface (second layer) of particle, respectively. This is a direct consequence of the strong surface potential (see Sec. IV). The surface segregation causes the core composition to deviate substantially from the equiatomic value (the smaller the particle, the larger deviation). Note that, in Fe-Pt, the comparatively weaker surface potential does not produce such a strong surface segregation and the core composition is still close to the equiatomic value.[20]

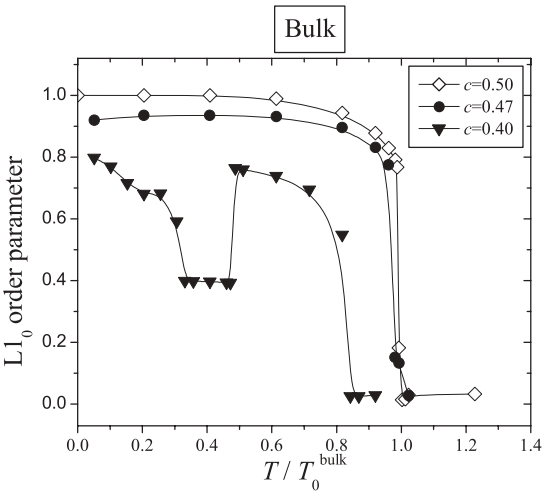

FIG. 8. Bulk $L1_0$ order parameter as a function of temperature obtained by Monte Carlo simulation at three atomic compositions $c = 0.5, 0.47, 0.4$.

The first effect of surface segregation on the total $L1_0$ order parameter follows from comparison of Figs. 9(a) and 9(b). Namely, the total $L1_0$ order of the particle is lower than that of the core. This is an obvious consequence of low $L1_0$ order in the two outer atomic layers due to the strong surface segregation. The effect is larger for smaller particles. For example, the difference between total and core $L1_0$ order is 31% and 77% for TO-10 and TO-3, respectively, at $T/T_0^{bulk} = 0.6$. This effect in Co-Pt is stronger than in Fe-Pt due to the stronger surface segregation.

The second effect of surface segregation on $L1_0$ order parameter is indirect. Figure 9(c) demonstrates that a considerable deviation of core composition from equiatomic value takes place for small particles at low temperatures. This deviation correlates with a substantial decrease of the $L1_0$ order parameter. We speculate that nonequiatomic composition within the core initiates order-order and/or decomposition phase transitions similar to bulk [compare Figs. 8 and 9(b)]. This effect is not observed in Fe-Pt nanoparticles[20] because the

TABLE VI. The characteristics of truncated octahedrons ("TO") used in Monte Carlo simulations. D_{100} is a diameter along the [100] direction. D_{sph} is a diameter of the spherical particle with the same volume (Ref. 22). D_{TO} is the distance between truncated octahedron corners along the diagonal (Ref. 20). N_{at} is the total number of atoms. c^{Pt}_{total} is the total Pt composition. $N^{surf}_{at}/N^{core}_{at}$ is the fraction of atoms at two external layers with respect to core. All diameters (in nm) are calculated assuming bulk lattice parameter $a_0 = 0.38$ nm. Note that the number of [100] atomic planes in a particle is even and equal to double value of D_{100} measured in a_0 units.

	D_{100} (a_0)	D_{100} (nm)	D_{sph} (nm)	D_{TO} (nm)	N_{at}	c^{Pt}_{total}	$\frac{N^{surf}_{at}}{N^{core}_{at}}$
TO-3	6	2.28	2.30	2.55	459	0.512	4.40
TO-4	8	3.04	3.25	3.40	1289	0.510	1.81
TO-5	10	3.80	3.81	4.25	2075	0.507	1.41
TO-7	14	5.32	5.31	5.95	5635	0.505	0.82
TO-10	20	7.60	7.76	8.50	17561	0.503	0.47

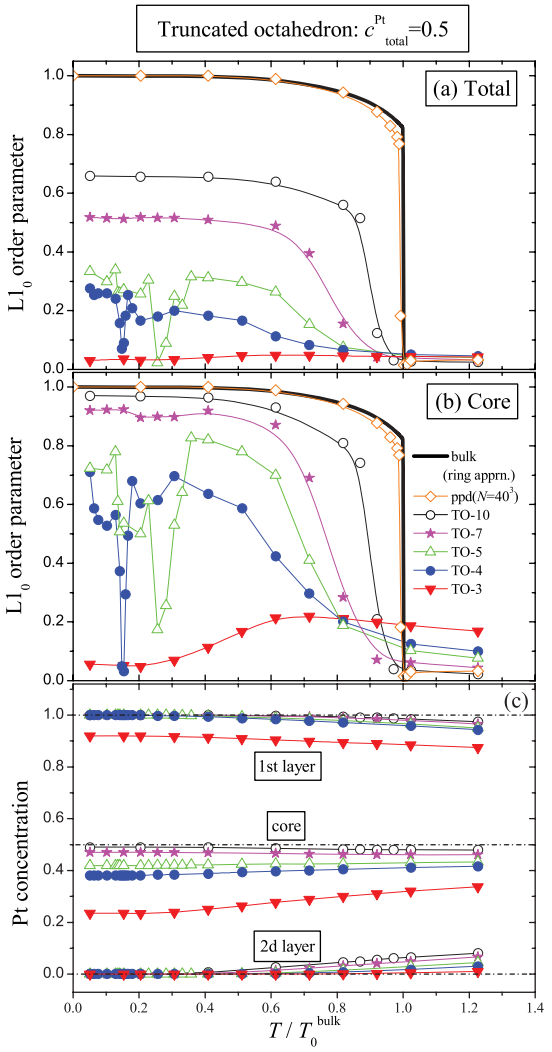

FIG. 9. (Color online) The temperature dependence of (a) total and (b) core equilibrium $L1_0$ order parameters $\overline{\eta}$ [Eq. (1)] as well as of (c) Pt concentrations (segregation profile) in two external layers and internal core for five truncated octahedrons ("TO") at near-equiatomic compositions (see Table VI). In graphs (a) and (b), we also include the data obtained by Monte Carlo simulation for the parallelepiped ("ppd") sample containing $N = 40^3$ atoms and by the analytical ring approximation (Refs. 73 and 74), both representing bulk at equiatomic composition. The core excludes two external layers of particle.

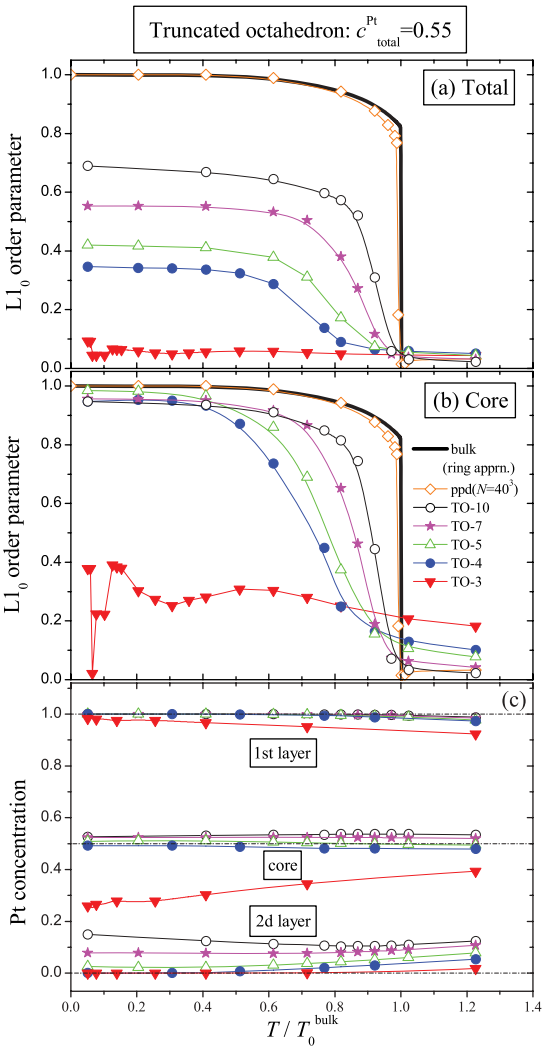

FIG. 10. (Color online) The same as in Fig. 9 but for all truncated octahedrons taken at total Pt composition $c = 0.55$.

corresponding surface segregation is not sufficiently strong to markedly change the core composition.

For further verification, we perform simulations for the same particles but with higher total composition $c = 0.55$ (see Fig. 10). Figure 10(c) shows that the implied increase of total Pt composition shifts the core composition closer to equiatomic value and increases the Pt composition in the second layer. Correspondingly, we get an increase of both core and total $L1_0$ order parameters for all particles. Only the core Pt composition of the smallest particle TO-3 is still far from equiatomic value. Accordingly, $L1_0$ order in TO-3 remains comparatively small, still showing signs of order-order and/or decomposition phase transition at low temperatures.

Remarkably, the composition effect on the $L1_0$ order can be even stronger than the effect of particle size. For example, the core $L1_0$ order in TO-5 particle is larger than in bigger particles TO-7 and TO-10 at low temperatures for $c = 0.55$ [Fig. 10(b)]. This is because the core Pt composition of the TO-5 particle is the closest to equiatomic value among all considered particles [see Fig. 9(c)].

The considered truncated octahedrons contain an even number of (100), (010), and (001) atomic planes (see Table VI). Thus, we are able to get complete $L1_0$ order at (near-) equiatomic composition. The consideration of an odd number of (100), (010), and (001) atomic planes[21,22] may be another possible way to cohere a high $L1_0$ order and surface segregation. It is out of this paper's scope, but deserves future consideration.

We avoid talking about the order-disorder transition temperature for such small particles because the transition is smeared and not well defined. Moreover, it is known (see Sec. 2.2.8 in Ref. 94) that there is no formal phase transition in a finite system. The experimental phase transition is often attributed to the lowest annealing temperature at which the ordered phase appears in a small particle. However, a temperature determined

in this way depends on kinetic properties as well as the relative free energies that determine equilibrium properties.

VI. CONCLUSIONS

For an accurate description of the configurational behavior of Co-Pt nanoparticles, both bulk and local (inhomogeneous) cluster expansions are calculated from first principles. Only two external layers of (001), (100), and (111) surfaces are found to be affected by surface potentials. A strong Pt and Co segregation to the first and second surface layers, respectively, is observed in Monte Carlo simulation of Co-Pt truncated octahedrons. So, the segregation takes a core/Co/Pt or "onion2shell" profile.[95–97]

The surface segregation produces a twofold effect on $L1_0$ atomic order. Directly, the $L1_0$ order in two surface layers is decreased due to the surface segregation, thus decreasing the total particle order as well. Indirectly, the surface segregation results in a depletion of Pt within the particle core in small Co-Pt nanoparticles. The depletion initiates a considerable drop of $L1_0$ order at low temperatures because of the adaptive character of the $L1_0$ structure on the fcc-restricted convex hull.[87] However, it is shown that the $L1_0$ order can be considerably restored by tuning the *total* composition of small particles.

According to the bulk global convex hull,[87] the hcp structure $B19$ is energetically degenerate with $L1_0$, and the phase separation into hcp $D0_{19}$ and fcc $\beta 2$ structures becomes more stable than $L1_0$ at low temperatures. So, below the fcc/hcp phase transition, another reason for $L1_0$ destruction may exist, if $L1_0$ is not stabilized kinetically.

The segregation tendencies in Co-Pt nanoparticles are similar to those of Fe-Pt,[20] but stronger. The large composition variation predicted here for Co-Pt is not predicted for the Fe-Pt particle core.[20] Another difference is the prediction that the $L1_0$ structure is a deep global ground state[98] in Fe-Pt rather than an adaptive fcc-restricted ground state as in Co-Pt. As a result, the equilibrium $L1_0$ order does not drop for low-temperature/small-size Fe-Pt equiatomic nanoparticles as we predict for Co-Pt.

The consideration of vibrational[75] and/or magnetic[50,99] degrees of freedom as well as the effect of particle substrate and polymeric interparticle medium are potential ways for improving the model we have used. In particular, they are necessary for more precise estimation of the temperature of bulk order-disorder transition. However, the calculated surface potential is so strong that the effect of particle environment should not be dominant (especially at the second surface atomic layer). In addition to the lattice contraction and change of particle shape due to surface tension,[93] the inclusion of effects of edges and corners,[100] kinetic factors and preparation conditions, as well as surface and core reconstructions[41,44,82,101–103] may be essential for precise treatment of very small particles.

The combination of the applied *ab initio* approach with nanofabrication techniques is a promising direction for designing new nanosystems with superior chemical, optical, and electronic properties.[104–110] For instance, the predicted strong Pt segregation in the external layer of Fe-Pt and Co-Pt nanoparticles may be important for applications by allowing nanoparticles to be produced at lower cost and higher oxidation and corrosion resistance. The results reported here may also be useful to those interested in understanding the transition from "macroscale physics" to "nanoscale physics."

ACKNOWLEDGMENT

Computational support was provided by the High Performance Computing (HPC) resources at the Center for Materials for Information Technology (University of Alabama, Tuscaloosa).

APPENDIX: ATOMIC COORDINATES OF THE STRUCTURES

Here, we show the description of those structures that are mentioned in the main text but have no known prototypes. Everywhere, $A = \mathrm{Co}$, $B = \mathrm{Pt}$.

Co_5Pt_4 (No. 37 in Table I)

This structure belongs to fcc-restricted convex hull of bulk Co-Pt.[87] The structure Co_4-Pt_5 (No. 39 in Table I) is isomorphic to this one.

Unit-cell basis vectors coordinates in Cartesian:
(1,0,0), (1/2,3/2,0), (1/2,0,3/2).
Atomic coordinates in Cartesian:
A: (1,1,0), (1/2,1,1/2), (1,0,1), (1/2,1/2,1), (1,1,1).
B: (0,0,0), (1/2,1/2,0), (1/2,0,1/2), (1,1/2,1/2).

Co_5Pt_4 (No. 39 in Table I)

The structure Co_4-Pt_5 (No. 40 in Table I) is isomorphic to this one.

Unit-cell basis vectors coordinates in Cartesian:
(1,0,0), (1/2,3/2,0), (1/2,0,3/2).
Atomic coordinates in Cartesian:
A: (1/2,1/2,0), (1,1,0), (1/2,0,1/2), (1/2,1/2,1), (1,1,1).
B: (0,0,0), (1,1/2,1/2), (1/2,1,1/2), (1,0,1).

Co_3Pt_9

This and the next three structures belong to a chain of $\beta 2$ derivatives that belong to the global bulk convex hull of Co-Pt or are very close to it.[87]

Unit-cell basis vectors coordinates in Cartesian:
(1,0,0), (1/2,3/2,0), (0,0,2).
Atomic coordinates in Cartesian:
A: (0,0,0), (1/2,0,1/2), (0,0,1).
B: (1/2,1/2,0), (1,1,0), (1,1/2,1/2), (1/2,1,1/2), (1/2,1/2,1), (1,1,1), (1/2,0,3/2), (1,1/2,3/2), (1/2,1,3/2).

Co_2Pt_7

Unit-cell basis vectors coordinates in Cartesian:
(1,0,0), (1/2,3/2,0), (1/2,0,3/2).
Atomic coordinates in Cartesian:
A: (0,0,0), (1/2,1/2,0).
B: (1,1,0), (1/2,0,1/2), (1,1/2,1/2), (1/2,1,1/2), (1,0,1), (1/2,1/2,1), (1,1,1).

$CoPt_5$

Unit-cell basis vectors coordinates in Cartesian:
(1,0,0), (0,1,0), (0,1/2,3/2).
Atomic coordinates in Cartesian:
A: (0,0,0).
B: (1/2,1/2,0), (1/2,1,1/2), (0,1/2,1/2), (0,1,1), (1/2,1/2,1).

Co_2Pt_{13}

Unit-cell basis vectors coordinates in Cartesian:
(1,0,0), (1/2,3/2,0), (1/2,0,5/2).
Atomic coordinates in Cartesian:
A: (0,0,0), (1,0,1).
B: (1/2,1/2,0), (1,1,0), (1/2,0,1/2), (1,1/2,1/2), (1/2,1,1/2), (1/2,1/2,1), (1,1,1), (1/2,0,3/2), (1,1/2,3/2), (3/2,1,3/2), (1,0,2), (3/2,1/2,2), (1,1,2).

---

*Present address: Grandis Inc., San Jose, California 95134, USA.

[1] *Binary Alloy Phase Diagrams*, edited by T. B. Massalski, H. Okamoto, P. R. Subramanian, and L. Kacprzak (American Society for Metals, Materials Park, OH, 1990).
[2] R. A. McCurrie and P. Gaunt, Philos. Mag. **13**, 567 (1966).
[3] S. Ostanin, S. Razee, J. Staunton, B. Ginatempo, and E. Bruno, J. Appl. Phys. **93**, 453 (2003).
[4] T. Burkert, O. Eriksson, S. I. Simak, A. V. Ruban, B. Sanyal, L. Nordström, and J. M. Wills, Phys. Rev. B **71**, 134411 (2005).
[5] Z. Lu, R. V. Chepulskii, and W. H. Butler, Phys. Rev. B **81**, 094437 (2010).
[6] S. Sun, C. B. Murray, D. Weller, L. Folks, and A. Moser, Science **287**, 1989 (2000).
[7] H. Zeng, J. Li, J. P. Liu, Z. L. Wang, and S. Sun, Nature (London) **420**, 395 (2002).
[8] Y. K. Takahashi, T. Ohkubo, M. Ohnuma, and K. Hono, J. Appl. Phys. **93**, 7166 (2003).
[9] T. Miyazaki, O. Kitakami, S. Okamoto, Y. Shimada, Z. Akase, Y. Murakami, D. Shindo, Y. K. Takahashi, and K. Hono, Phys. Rev. B **72**, 144419 (2005).
[10] F. Baletto and R. Ferrando, Rev. Mod. Phys. **77**, 371 (2005).
[11] S. Sun, Adv. Mater. **18**, 393 (2006).
[12] S. Bader, Rev. Mod. Phys. **78**, 1 (2006).
[13] C.-b. Rong, D. Li, V. Nandwana, N. Poudyal, Y. Ding, Z. L. Wang, H. Zeng, and J. P. Liu Adv. Mater. **18**, 2984 (2006).
[14] J. R. Liu, K. Elkins, D. Li, V. Nandwana, and N. Poudyal, IEEE Trans. Magn. **42**, 3036 (2006).
[15] S. Kang, S. Shi, Z. Jia, G. B. Thompson, D. E. Nikles, J. W. Harrell, D. Li, N. Poudyal, V. Nandwana, and J. P. Liu, J. Appl. Phys. **101**, 09J113 (2007).
[16] U. Wiedwald, A. Klimmer, B. Kern, L. Han, H. G. Boyen, P. Ziemann, and K. Fauth, Appl. Phys. Lett. **90**, 062508 (2007).
[17] R. Ferrando, J. Jellinek, and R. L. Johnston, Chem. Rev. **108**, 845 (2008).
[18] R. V. Chepulskii, J. Velev, and W. H. Butler, J. Appl. Phys. **97**, 10J311 (2005).
[19] R. V. Chepulskii and W. H. Butler, Phys. Rev. B **72**, 134205 (2005).
[20] R. V. Chepulskii, W. H. Butler, A. van de Walle, and S. Curtarolo, Scr. Mater. **62**, 179 (2010).
[21] B. Yang, M. Asta, O. Mryasov, T. Klemmer, and R. Chantrell, Scr. Mater. **53**, 417 (2005).
[22] B. Yang, M. Asta, O. N. Mryasov, T. J. Klemmer, and R. W. Chantrell, Acta Mater. **54**, 4201 (2006).
[23] M. Müller and K. Albe, Phys. Rev. B **72**, 094203 (2005).
[24] M. Müller, P. Erhart, and K. Albe, Phys. Rev. B **76**, 155412 (2007).
[25] G. Rossi, R. Ferrando, and C. Mottet, Faraday Discuss. **138**, 193 (2008).
[26] D. Alloyeau, C. Ricolleau, C. Mottet, T. Oikawa, C. Langlois, Y. Le Bouar, N. Braidy, and A. Loiseau, Nat. Mater. **8**, 940 (2009).
[27] X. Sun, Z. Y. Jia, Y. H. Huang, J. W. Harrell, D. E. Nikles, K. Sun, and L. M. Wang, J. Appl. Phys. **95**, 6747 (2004).
[28] A. Hannour, L. Bardotti, B. Prèvel, E. Bernstein, P. Mèlinon, A. Perez, J. Gierak, E. Bourhis, and D. Mailly, Surf. Sci. **594**, 1 (2005).
[29] M. Mizuno, Y. Sasaki, M. Inoue, C. N. Chinnasamy, B. Jeyadevan, D. Hasegawa, T. Ogawa, M. Takahashi, K. Tohji, K. Sato *et al.*, J. Appl. Phys. **97**, 10J301 (2005).
[30] L. Castaldi, K. Giannakopoulos, A. Travlos, D. Niarchos, S. Boukari, and E. Beaurepaire, J. Magn. Magn. Mater. **290-291**, 544 (2005).
[31] D. Alloyeau, C. Langlois, C. Ricolleau, Y. L. Bouar, and A. Loiseau, Nanotechnology **18**, 375301 (2007).
[32] J. H. Kim, J. Kim, N. Oh, Y.-H. Kim, C. K. Kim, C. S. Yoon, and S. Jin, Appl. Phys. Lett. **90**, 023117 (2007).
[33] F. Tournus, A. Tamion, N. Blanc, A. Hannour, L. Bardotti, B. Prével, P. Ohresser, E. Bonet, T. Epicier, and V. Dupuis, Phys. Rev. B **77**, 144411 (2008).
[34] C. Langlois, D. Alloyeau, Y. Le Bouar, A. Loiseau, T. Oikawa, C. Mottet, and C. Ricolleau, Faraday Discuss. **138**, 375 (2008).
[35] N. Blanc, F. Tournus, V. Dupuis, and T. Epicier, Phys. Rev. B **83**, 092403 (2011).
[36] Y. Gauthier, R. Baudoing-Savois, J. Bugnard, U. Bardi, and A. Atrei, Surf. Sci. **276**, 1 (1992).
[37] A. V. Ruban, H. L. Skriver, and J. K. Nørskov, Phys. Rev. B **59**, 15990 (1999).
[38] Y. Chui and K. Chan, Chem. Phys. Lett. **408**, 49 (2005).
[39] S. Heinrichs, W. Dieterich, and P. Maass, Europhys. Lett. **75**, 167 (2006).
[40] O. Ersen, C. Goyhenex, and V. Pierron-Bohnes, Phys. Rev. B **78**, 035429 (2008).
[41] M. E. Gruner, J. Phys.: Conf. Ser. **200**, 072039 (2010).
[42] A. U. Nilekar, A. V. Ruban, and M. Mavrikakis, Surf. Sci. **603**, 91 (2009).
[43] L.-L. Wang and D. D. Johnson, J. Am. Chem. Soc. **131**, 14023 (2009).
[44] M. E. Gruner, J. Phys. D: Appl. Phys. **43**, 474008 (2010).
[45] L. Qin, Y. Zhang, S. Huang, H. Tian, and P. Wang, Phys. Rev. B **82**, 075413 (2010).
[46] F. Calvo and C. Mottet, Phys. Rev. B **84**, 035409 (2011).
[47] C. Leroux, M. C. Cadeville, V. Pierron-Bohnes, G. Inden, and F. Hinz, J. Phys. F: Met. Phys. **18**, 2033 (1988).
[48] C. Leroux, A. Loiseau, D. Broddin, and G. Vantendeloo, Philos. Mag. B **64**, 57 (1991).
[49] H. Okamoto, J. Phase Equilib. **22**, 591 (2001).

[50] A. Alam, B. Kraczek, and D. D. Johnson, Phys. Rev. B **82**, 024435 (2010).
[51] W. Qi, Y. Li, S. Xiong, and S.-T. Lee, Small **6**, 1996 (2010).
[52] J. M. Sanchez, F. Ducastelle, and D. Gratias, Phys. A (Amsterdam) **128**, 334 (1984).
[53] D. D. Fontaine, *Cluster Approach to Order-Disorder Transformations in Alloys*, Vol. 47 of Solid State Physics (Academic, New York, 1994).
[54] G. L. W. Hart, V. Blum, M. J. Walorski, and A. Zunger, Nat. Mater. **4**, 391 (2005).
[55] A. van de Walle and G. Ceder, J. Phase Equilib. **23**, 348 (2002).
[56] R. Drautz, H. Reichert, M. Fähnle, H. Dosch, and J. M. Sanchez, Phys. Rev. Lett. **87**, 236102 (2001).
[57] A. Van der Ven, G. Ceder, M. Asta, and P. D. Tepesch, Phys. Rev. B **64**, 184307 (2001).
[58] A. Van der Ven and G. Ceder, Phys. Rev. B **71**, 054102 (2005).
[59] J. P. Perdew, K. Burke, and M. Ernzerhof, Phys. Rev. Lett. **77**, 3865 (1996).
[60] G. Kresse and J. Furthmuller, Comput. Mater. Sci. **6**, 15 (1996).
[61] M. Methfessel and A. T. Paxton, Phys. Rev. B **40**, 3616 (1989).
[62] T. D. Lee and C. N. Yang, Phys. Rev. **87**, 410 (1952).
[63] M. A. Krivoglaz and A. A. Smirnov, *The Theory of Order-Disorder in Alloys* (Macdonald, Materials Park, London, 1964).
[64] A. G. Khachaturyan, Prog. Mater. Sci. **22**, 1 (1978).
[65] D. D. Fontaine, *Configurational Thermodynamics of Solid Solutions*, Vol. 34 of Solid State Physics (Academic, New York, 1979).
[66] F. Ducastelle, *Order and Phase Stability in Alloys* (Elsevier, New York, 1991).
[67] M. Asta, C. Wolverton, D. de Fontaine, and H. Dreyssé, Phys. Rev. B **44**, 4907 (1991).
[68] C. Wolverton, M. Asta, H. Dreyssé, and D. de Fontaine, Phys. Rev. B **44**, 4914 (1991).
[69] N. A. Zarkevich, D. D. Johnson, and A. V. Smirnov, Acta Mater. **50**, 2443 (2002).
[70] N. I. Vlasova, G. S. Kandaurova, and N. N. Shchegoleva, J. Magn. Magn. Mater. **222**, 138 (2000).
[71] R. Hultgren, P. D. Desai, D. T. Hawkins, M. Gleiser, and K. K. Kelley, *Selected Values of Thermodynamic Properties of Binary Alloys* (American Society for Metals, Metals Park, Ohio, 1973).
[72] R. V. Chepulskii, S. V. Barabash, and A. Zunger, Phys. Rev. B **85**, 144201 (2012).
[73] R. V. Chepulskii, Solid State Commun. **115**, 497 (2000).
[74] R. V. Chepulskii, Phys. Rev. B **69**, 134431 (2004).
[75] A. van de Walle and G. Ceder, Rev. Mod. Phys. **74**, 11 (2002).
[76] B. Fultz, Prog. Mater. Sci. **55**, 247 (2010).
[77] R. V. Chepulskii, J. Phys.: Condens. Matter **10**, 1505 (1998).
[78] S. I. Park, B. J. Lee, and H. M. Lee, Scr. Mater. **45**, 495 (2001).
[79] M. Allalen, H. Bouzar, and T. Mehaddene, Eur. Phys. J. B **45**, 443 (2005).
[80] P. Moskovkin and M. Hou, J. Alloys Compd. **434-435**, 550 (2007).
[81] P. Moskovkin, S. Pisov, M. Hou, C. Raufast, F. Tournus, L. Favre, and V. Dupuis, Eur. Phys. J. D **43**, 27 (2007).
[82] P. Andreazza, C. Mottet, C. Andreazza-Vignolle, J. Penuelas, H. C. N. Tolentino, M. De Santis, R. Felici, and N. Bouet, Phys. Rev. B **82**, 155453 (2010).
[83] H. Reichert, S. C. Moss, and K. S. Liang, Phys. Rev. Lett. **77**, 4382 (1996).
[84] D. K. Saha, K. Koga, and K. Ohshima, J. Phys.: Condens. Matter **4**, 10093 (1992).
[85] R. V. Chepulskii, J. B. Staunton, E. Bruno, B. Ginatempo, and D. D. Johnson, Phys. Rev. B **65**, 064201 (2001).
[86] R. V. Chepulskii, J. Phys.: Condens. Matter **14**, L193 (2002).
[87] R. V. Chepulskii and S. Curtarolo, Appl. Phys. Lett. **99**, 261902 (2011).
[88] I. Billas, A. Chatelain, and W. Deheer, Science **265**, 1682 (1994).
[89] M. L. Tiago, Y. Zhou, M. M. G. Alemany, Y. Saad, and J. R. Chelikowsky, Phys. Rev. Lett. **97**, 147201 (2006).
[90] L. D. Marks, Rep. Prog. Phys. **57**, 603 (1994).
[91] M. J. Yacaman, J. A. Ascencio, H. B. Liu, and J. Gardea-Torresdey, J. Vac. Sci. Technol. B **19**, 1091 (2001).
[92] Z. R. Dai, S. Sun, and Z. L. Wang, Surf. Sci. **505**, 325 (2002).
[93] R. V. Chepulskii and S. Curtarolo, ACS Nano **5**, 247 (2011).
[94] O. G. Mouritsen, *Computer Studies of Phase Transitions and Critical Phenomena* (Springer, Berlin, 1984).
[95] B.-J. Hwang, L. S. Sarma, J.-M. Chen, C.-H. Chen, S.-C. Shih, G.-R. Wang, D.-G. Liu, J.-F. Lee, and M.-T. Tang, J. Am. Chem. Soc. **127**, 11140 (2005).
[96] D. Cheng, W. Wang, and S. Huang, J. Phys. Chem. B **110**, 16193 (2006).
[97] D. Cheng and D. Cao, Chem. Phys. Lett. **461**, 71 (2008).
[98] S. V. Barabash, R. V. Chepulskii, V. Blum, and A. Zunger, Phys. Rev. B **80**, 220201 (2009).
[99] A. V. Ruban and I. A. Abrikosov, Rep. Prog. Phys. **71**, 046501 (2008).
[100] A. S. Barnard and P. Zapol, J. Chem. Phys. **121**, 4276 (2004).
[101] M. Müller and K. Albe, Acta Mater. **55**, 6617 (2007).
[102] M. E. Gruner, G. Rollmann, P. Entel, and M. Farle, Phys. Rev. Lett. **100**, 087203 (2008).
[103] J. Penuelas, P. Andreazza, C. Andreazza-Vignolle, H. C. N. Tolentino, M. De Santis, and C. Mottet, Phys. Rev. Lett. **100**, 115502 (2008).
[104] J. Greeley and M. Mavrikakis, Nat. Mater. **3**, 810 (2004).
[105] S. Alayoglu, A. U. Nilekar, M. Mavrikakis, and B. Eichhorn, Nat. Mater. **7**, 333 (2008).
[106] J. K. Nørskov, T. Bligaard, J. Rossmeisl, and C. H. Christensen, Nat. Chem. **1**, 37 (2009).
[107] J. K. Nørskov and F. Abild-Pedersen, Nature (London) **461**, 1223 (2009).
[108] J. Greeley, I. E. L. Stephens, A. S. Bondarenko, T. P. Johansson, H. A. Hansen, T. F. Jaramillo, J. Rossmeisl, I. Chorkendorff, and J. K. Nørskov, Nat. Chem. **1**, 552 (2009).
[109] K. J. J. Mayrhofer and M. Arenz, Nat. Chem. **1**, 518 (2009).
[110] Y. Gauthier, M. Schmid, S. Padovani, E. Lundgren, V. Bus, G. Kresse, J. Redinger, and P. Varga, Phys. Rev. Lett. **87**, 036103 (2001).